 CMC, vol.1, no.1, pp.51-58, 2004

The Effect of the Reynolds Number on Lateral Migration of Nonneutrally-Buoyant Spherical Particles in Poiseuille Flow

S.-C. Hsiao[1] **and M.S. Ingber**[2]

Abstract: The lateral migration of nonneutrally-buoyant spherical particles in Poiseuille flow is investigated numerically using the boundary element method. In particular, the steady, Navier-Stokes equations are solved using a classical domain integration method treating the nonlinear terms as pseudo-body forces. The numerical results for the lateral migration velocity are compared with experimental data [Jeffrey and Pearson (1963)]. The numerical results indicate that the lateral migration velocity does not scale linearly with the Reynolds number. The methodology is extended to include non-Newtonian power-law fluids. The migration velocity is significantly affected for particles suspended in this class of fluids and can actually change direction for large values of the power-law index.

keyword: lateral migration, low Reynolds number flow, non-Newtonian fluids, boundary element method.

1 Introduction

Particles suspended in pressure-driven flows play an important role in many engineering applications such as secondary petroleum recovery processes, paper manufacturing, chromotography, environmental waste treatment, and composite material processing. As a result, many analytical and experimental studies have been performed to characterize particle behavior in nonlinear shear flows [Segré and Silberberg (1961); Ho and Leal (1974); Jeffrey and Pearson (1963); Cox and Hsu (1977); Vasseur and Cox (1976a); Vasseur and Cox (1976b)]. In addition, several numerical studies have been performed for this class of flows based on traditional boundary element methods both in the zero-Reynolds number limit [Ingber (1991); Tran-Cong and Phan-Thien (1989); Fang, Mammoli, and Ingber (2001)] and at low, but finite, Reynolds numbers [Li and Ingber (1994)]. Recently, a class of meshless methods have been developed which can be applied to this problem both in the zero-Reynolds number limit [Tsai, Young, and Cheng (2002)] and at finite Reynolds number [Lin and Atluri (2001)].

Spheres at low but nonzero Reynolds number experience a radial force which results in a lateral migration velocity in cylindrical Poiseuille flow. In fact, in many cases, particles tend to accumulate in preferential radial locations within the cylinder which may be a desired result (e.g., chromotography) or an undesired result (e.g., composite materials processing). The lateral migration velocity is several orders of magnitude smaller than the characteristic Poiseuille mean flow velocity making it is extremely difficult to obtain accurate quantitative experimental results. Therefore, it is not surprising that the existing experimental data which was collected more than two decades ago show considerable scatter [Ishii and Hasimoto (1980)]. Alternatively, numerical experiments for well-characterized systems can be efficiently performed. Li and Ingber (1994) investigated the lateral migration of spherical particles in Poiseuille flow using the boundary element method. To avoid the domain integration associated with the nonlinear convective acceleration term, a particular solution method similar to the dual reciprocity method was used. Two cases were considered for nonneutrally-buoyant spheres in Poiseuille flow, namely, the case in which the sphere lags the mean flow and the case in which the sphere leads the mean flow. Although their results show reasonable agreement with experimental results, the lateral migration velocity for particles near the center of the cylinder showed the opposite sign compared to experiment for both the lead and lag cases.

An alternative approach for dealing with the nonlinear convective acceleration term is the direct domain integration method which is adopted in this study. In particular, the lateral migration problem is investigated with particular attention being paid to the effect of the Reynolds number on the migration velocity. The extension of the

[1] National Cheng Kung University, Tainan, Taiwan.
[2] University of New Mexico, Albuquerque, NM, USA.

BEM methodology using direct domain integration to non-Newtonian fluids is straight forward since the extra stress simply becomes an additional term in the domain integral. Non-Newtonian power-law fluids are also considered in the current study. The numerical methodology is presented in Section 2, results are presented in Section 3, and conclusions are presented in Section 4.

2 Numerical formulation for Newtonian and non-Newtonian fluids

The system under consideration in this study consists of a nonneutrally-buoyant sphere of radius a suspended in an incompressible Poiseuille flow at a distance b from the axis of the cylinder (Fig. 1). It is well known that the system is characterized by the quasi-steady Navier-Stokes equations given in tensor form by

$$-\frac{\partial p(x)}{\partial x_i}+\frac{\partial}{\partial x_j}\left[\eta\left(\frac{\partial u_i(x)}{\partial x_j}+\frac{\partial u_j(x)}{\partial x_i}\right)\right]=\rho_f u_j(x)\frac{\partial u_i(x)}{\partial x_j} \tag{1}$$

$$\frac{\partial u_j(x)}{\partial x_j}=0 \tag{2}$$

where p is the pressure, η is the dynamic viscosity, u_i is the component of the velocity vector and ρ_f is the density of fluid.

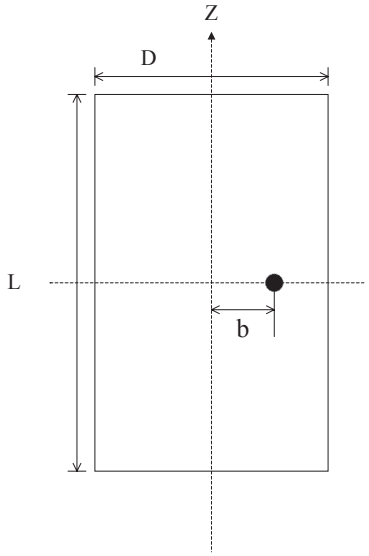

Figure 1 : A sketch of the problem geometry.

A power-law model [Chhabra (1993)] is adopted in this study whereby the viscosity, η, is a function of the shear rate, $\dot{\gamma}$, given by

$$\eta(\dot{\gamma})=K\dot{\gamma}^{n-1} \tag{3}$$

where K is called the consistency index, $0<n\leq 1$ is the power-law index, and $\dot{\gamma}$ is the generalized shear rate defined by

$$\dot{\gamma}=\sqrt{2\varepsilon_{ij}\varepsilon_{ij}} \tag{4}$$

where ε_{ij} is the rate of strain tensor given by

$$\varepsilon_{ij}=\frac{1}{2}\left(\frac{\partial u_i}{\partial x_j}+\frac{\partial u_j}{\partial x_i}\right) \tag{5}$$

It is noted that the power-law model reduces to the Newtonian case by choosing $n=1$.

The stress tensor and the deviatoric stress tensor for the power-law fluid can be written as

$$\sigma_{ij}=-p\delta_{ij}+\tau_{ij}$$
$$\tau_{ij}=2\eta(\dot{\gamma})\varepsilon_{ij} \tag{6}$$

Assuming that the non-Newtonian fluid property does not deviate much from the "base Newtonian" fluid, the stress tensor can be decomposed into a linear part, $\tau_{ij}^{(N)}$, and a nonlinear part, $\tau_{ij}^{(e)}$. The nonlinear part, $\tau_{ij}^{(e)}$, is commonly referred to as the "extra stress". Hence, the stress tensor can be written as

$$\sigma_{ij}=-p\delta_{ij}+\eta_N\varepsilon_{ij}+\tau_{ij}^{(e)}=\sigma_{ij}^{(N)}+\tau_{ij}^{(e)} \tag{7}$$

where

$$\sigma_{ij}^{(N)}=-p\delta_{ij}+\eta_N\varepsilon_{ij}$$
$$\tau_{ij}^{(e)}=(\eta(\dot{\gamma})-\eta_N)\varepsilon_{ij} \tag{8}$$

where η_N is a free constant which can be chosen to be the zero-shear rate viscosity.

The boundary conditions on the lateral surface of the cylinder are given by the no slip conditions and the boundary conditions on the top and bottom of the cylinder are prescribed by the undisturbed Poiseuille flow velocity. That is, it is assumed that the disturbance caused by the particle at both ends of cylinder is negligible. It is possible to prescribe pressure boundary conditions on the ends of the cylinder but this introduces a hypersingular integral into the boundary element formulation [Ingber and Li (1991)]. Along the boundary of the particle, the no-slip boundary condition is given by

$$u_i=u_i^c+\varepsilon_{ijk}\omega_j r_k \tag{9}$$

where u_i^c is the centroidal component of the particle velocity, ε_{ijk} is the permutation symbol, ω_j is the centroidal component of the particle angular velocity and r_k is the position vector component from the centroid of the particle to the boundary.

To complete the problem description, the particle is assumed to be in equilibrium. That is, the only acceleration that is considered in the formulation is the convective fluid acceleration. The equilibrium equations for the particle can be written as

$$\int_{\Gamma_m} t_i d\Gamma - b_i = 0 \tag{10}$$

and

$$\int_{\Gamma_m} \varepsilon_{ijk} r_j t_k d\Gamma = 0 \tag{11}$$

where Γ_m is the surface of the particle and b_i is the component of the body force acting on the particle. Physically, these equations represent the force and moment balance for the particle. It is interesting to note that the rate of strain tensor, ε_{ij}, is zero on the particle surface as seen by substituting Eq. 9 into Eq. 5. Therefore the force and moment balances, Eq. 10 and Eq. 11, respectively, can be rewritten as

$$\int_{\Gamma_m} t_i^{(N)} d\Gamma - b_i = 0 \tag{12}$$

and

$$\int_{\Gamma_m} \varepsilon_{ijk} r_j t_k^{(N)} d\Gamma = 0 \tag{13}$$

where $t_i^{(N)}$ is the component of the Newtonian-based traction associated with $\sigma_{ij}^{(N)}$.

The governing differential equations (Eqs. 1 and 2) can be converted into a boundary integral equation using standard techniques [Ladyzhenskaya (1963)]. The corresponding boundary integral equation is given by

$$C_{ik}(x)u_i(x) + \int_\Gamma q_{ijk}^*(x,y)u_i(y)n_j(y)d\Gamma + \int_\Gamma u_{ik}^*(x,y)t_i^{(N)}(y)d\Gamma = -\int_\Omega u_{ik}^*(x,y)\, f_i(y)d\Omega \tag{14}$$

where

$$q_{ijk}^* = \frac{3(x_i-y_i)(x_j-y_j)(x_k-y_k)}{4\pi|x-y|^5},$$

$$u_{ik}^* = -\frac{1}{8\pi\mu}\left[\frac{\delta_{ik}}{|x-y|} + \frac{(x_i-y_i)(x_k-y_k)}{|x-y|^3}\right],$$

$$f_i = \rho_f u_j(x)\frac{\partial u_i(x)}{\partial x_j} - \frac{\partial \tau_{ij}^{(e)}}{\partial x_j},$$

Ω is a multiply-connected domain consisting of a circular tube with a spherical exclusion, Γ denotes the boundary of the domain Ω, δ_{ik} is the Kronecker-delta function, x_i is the component of the field point x and y_i is the component of the source point y. The coefficient tensor C_{ik} is related to the local geometry at the field point and can be computed using

$$C_{ik}(x) = -\int_\Gamma q_{ijk}^*(x,y)n_j(y)d\Gamma \tag{15}$$

The nonlinear convective acceleration and extra stress terms in Eq. 14 given by f_i appear in the domain integral as a pseudo-body force. It is worth noting that the pseudo-body force component, f_i, can be calculated at each Gauss point as long as the components of the velocity and the velocity gradient are known at the finite element nodes associated with the interior discretization. Several methods have been developed over the past several years to treat domain integrals in boundary element formulations including dual reciprocity methods [Partridge and Wrobel (1992); Golberg, Chen, Bowman, and Power (1998)], multiple reciprocity methods [Nowak (1989); Power (1994)], and particular solution methods [Ahmad and Banerjee (1986); Ingber and Phan-Thien (1992)]. In all of these methods, the domain integral can either be eliminated by constructing an approximate particular solution or the domain integral can be converted into a series of additional boundary integrals. These methods have been very popular in the boundary element literature, in part, for aesthetic reasons in that the analysis depends only on boundary integrals. Recently, however, Ingber, Mammoli, and Brown (2001) have shown that evaluating the domain integral in boundary element analyses using classical Gaussian quadrature can be, in many cases, more efficient than the above mentioned boundary only methods both in terms of accuracy and CPU requirements.

In the current formulation, classical Gaussian integration is used to evaluate the domain integral containing the nonlinear pseudo-body force terms. More specifically, the domain Ω is discretized into 10-node tetrahedral finite elements and the boundary of the domain Γ is discretized into superparametric quadrilateral boundary elements. In particular, the geometry is approximated

with biquadratic shape functions while the components of traction and velocity are approximated as constants within the boundary elements.

An incremental iteration scheme is used to evaluate the interior convective accelerations contained in the function f_i. Initially, for the first Reynolds number considered ($Re = 5$), the interior velocity and velocity gradient components are assumed to be zero. That is, the Stokes problem is solved. Then the boundary integral equation (BIE) (Eq. 14) is used to determine the interior velocity components and the derivative of the boundary integral equation (DBIE) is used to determine the interior velocity gradient terms. The interior domain integral is now evaluated with the updated convective acceleration terms and the boundary element analysis is again performed to determine the boundary unknowns. With the updated boundary data, the interior convective acceleration terms are evaluated using the BIE and DBIE. This process is repeated until the unknown data (centroidal linear and angular velocity components and boundary tractions) converge. The convergence criterion is given by

$$\frac{|d_{new} - d_{old}|}{d_{old}} < 5 \times 10^{-5} \tag{16}$$

where d is the vector comprised of the unknown data. Over-relaxation is used to accelerate the convergence of the iteration. Typically, convergent solutions were obtained within 20 iterations. Finally, in the incremental scheme, when going to the next higher Reynolds number, the converged solution for the previous Reynolds number is used initially to evaluate the domain integral containing the convective acceleration terms.

3 Results

Two cases are considered in this study for nonneutrally buoyant particles suspended in Poiseuille flow of a Newtonian fluid. The first case consists of either a heavy particle in an upflow or a buoyant particle in a downflow for which the particle lags the mean flow. The second case consists of either a heavy particle in a downflow or a buoyant particle in an upflow for which the particle leads the mean flow. The main focus of this study is on the relationship between lateral migration velocity, U_l, the Reynolds number, Re, and the eccentric position of the sphere, b. In addition, the case in which the particle leads the mean flow is considered for a power-law fluid.

3.1 Newtonian suspending fluid

The dimensionless parameters characterizing this problem are defined as

$$Re = \frac{\rho_f U_m D}{\mu}; \qquad Re_f = \frac{\rho_f U_\infty a}{\mu};$$
$$k = \frac{2a}{D}; \qquad r = \frac{2b}{D} \tag{17}$$

where Re is the tube Reynolds number, ρ_f is the fluid density, U_m is the mean velocity of the undisturbed Poiseuille flow, k is the ratio of the particle to cylinder diameter, Re_f is the particle free fall Reynolds number, and U_∞ is the sedimentation velocity of the sphere in an unbounded quiescent fluid. The sedimentation velocity is given by

$$U_\infty = \frac{2a^2(\rho_s - \rho_f)g}{9\mu} \tag{18}$$

in which ρ_s is the density of spherical particle and g is the gravitational constant.

The diameter of the tube D and the length L are taken to be 10 and 15, respectively in all of the following numerical results. After a series of convergence tests were performed, a discretization containing 224 boundary elements for the cylinder and 96 boundary elements for the sphere was used to generate the numerical results. In order to compare to the experimental results of Jeffrey and Pearson (1963), the parameter k is chosen to be $k = 0.09$ and $U_\infty/U_m = 0.14391$. Note that the parameter U_∞/U_m is essentially a measure of the density difference between the sphere and the suspending fluid.

Results for the lateral migration velocity U_l as a function of the dimensionless eccentric position, r, are plotted in Fig. 2 for the case where the particle leads the mean flow and in Fig. 3 for the case where the particle lags the mean flow. The lateral velocity is made dimensionless by dividing by $U_m Re$ to match the results of Jeffrey and Pearson (1963). Jeffrey and Pearson measured the tube Reynolds number to be $Re \approx 22.7$ in their experiments. It is seen in Fig. 2, for the case where the particle leads the mean flow, that the present numerical results for the lateral migration velocity are in satisfactory agreement with the experimental results. In particular, the numerical results are below the experimental results for $r < 0.65$ and are above the experimental results for $r > 0.65$. However, it should be noted that Jeffrey and Pearson did not

discuss, to any extent, experimental errors, and, in fact, state that "the results cannot be more than indicative of the quantitative nature of the general particle migration." Experimental measurements are difficult because the lateral migration velocity is several orders of magnitude less than the mean flow velocity, and hence, experimental errors may have been fairly large. Similar agreement between the current numerical results and experiment can be seen in Fig. 3 for the case where the particle lags the mean flow. Here, the numerical results are above (in absolute value) the experimental results for $r < 0.5$ and are below the experimental results for $r > 0.55$.

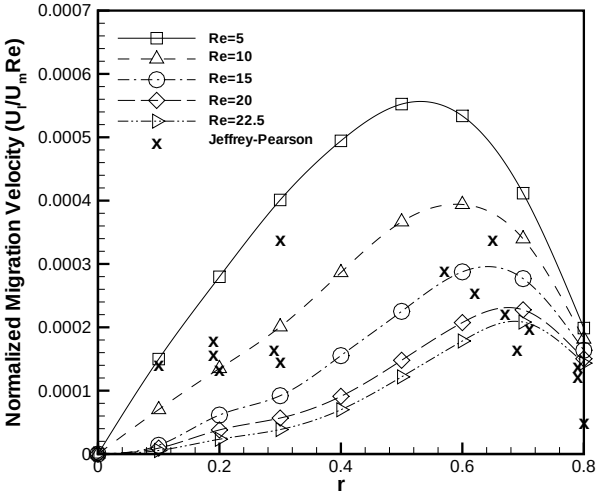

Figure 2 : The normalized lateral migration velocity as a function of the eccentric position r for the case in which the sphere leads the mean flow with U_∞/U_m=0.14391.

The dimensionless lateral velocity used by Jeffrey and Pearson as shown in Figs. 2 and 3 masks the dependence of the lateral migration velocity on the Reynolds number. In order to view this dependence more clearly, the lateral migration velocity is plotted against eccentric position in Figs. 4 and 5 for the cases in which the sphere leads and lags the mean velocity, respectively. The following observations can be made for both cases. At small eccentric positions, the absolute value of the lateral migration velocity decreases with Reynolds number whereas, at large eccentric positions, the absolute value of the lateral migration velocity increases with Reynolds number. At intermediate eccentric positions, the absolute value of

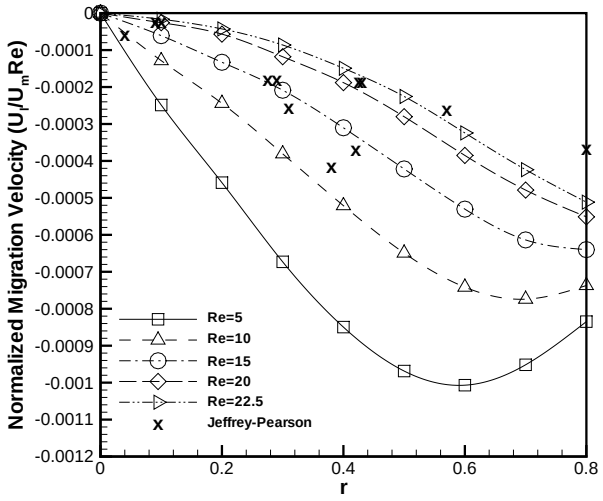

Figure 3 : The normalized lateral migration velocity as a function of the eccentric position r for the case in which the sphere lags the mean flow with U_∞/U_m=0.14391.

the migration velocity first increases then decreases with Reynolds number.

3.2 Power-law susupending fluid

To show the extension of the general methodology to a non-Newtonian fluid, a sphere suspended in tubular pressure-driven flow of a power-law fluid is considered. In particular, the case in which the particle leads the fluid velocity is considered for power-law indices in the range $0.4 \leq n \leq 0.9$. Again, it is assumed that the velocity disturbance at both ends of cylinder caused by the particle is negligible. The exact solution for the pressure-driven flow of a power-law fluid in a cylinder can be easily obtained by integrating radial momentum equation. The only non-zero velocity is a function of r and can be expressed as

$$u(r) = \frac{n}{n+1}\left(\frac{2}{K}\right)^{\frac{1}{n}}\left(-\frac{dp}{dz}\right)^{\frac{1}{n}}\left(\frac{D}{2}\right)^{\frac{n+1}{n}}\left(1-r^{\frac{n+1}{n}}\right) \quad (19)$$

or equivalently expressed in terms of average velocity U_m as

$$u(r) = \frac{3n+1}{n+1}U_m\left(1-r^{\frac{n+1}{n}}\right) \quad (20)$$

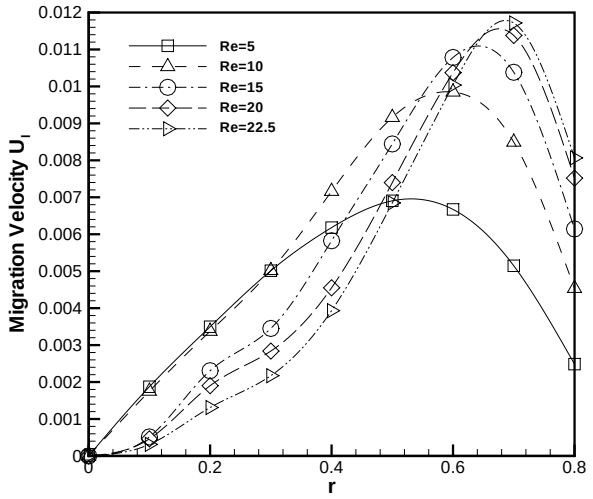

Figure 4 : The lateral migration velocity as a function of the eccentric position r for the case in which the sphere leads the mean flow with $|U_\infty|/U_m$=0.14391.

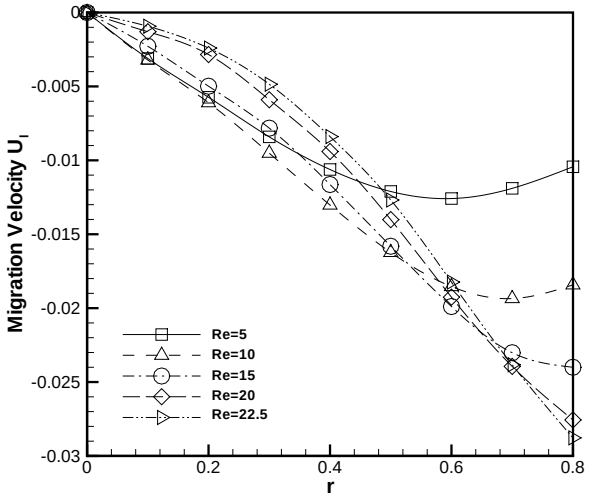

Figure 5 : The lateral migration velocity as a function of the eccentric position r for the case in which the sphere lags the mean flow with $|U_\infty|/U_m$=0.14391.

The corresponding pressure gradient is given by

$$-\frac{dp}{dz} = \left(\frac{3n+1}{n+1}\right)^n U_m^n \left(\frac{K}{2}\right)\left(\frac{D}{2}\right)^{-1-n} \tag{21}$$

Note that for fixed "r" and "U_m", the undisturbed velocity is only function of n which can be seen from Eqn. 20.

The initial position of the particle, consistency index, and Reynolds number are chosen as $r = 0.7$, $K = 5$, and $Re = 5$. In order to compare the non-Newtonian results with the Newtonian results, $k = 0.09$ and $U_\infty/U_m = 0.14391$. The lateral migration velocity as a function of the power-law index is shown in Fig. 6. The effect of reducing the power-law index from 1 (Newtonian case) is to reduce the lateral migration velocity. In fact, the direction of the migration velocity is seen to reverse as the power-law index is reduced below approximately 0.7.

4 Conclusions

The lateral migration of a rigid spherical particle in cylindrical Poiseuille flow is reexamined using the boundary element method with classical domain integration. The current numerical results are in good agreement with the experimental results of Jeffrey and Person (1963). Particular attention is paid to the effect of the Reynolds number on the migration velocity. Dimensional analysis indicates that the lateral velocity of the sphere, U_l, can be written as a function of the following parameters

$$\frac{U_l}{U_m} = f\left(Re, k, r, \frac{U_\infty}{U_m}\right) \tag{22}$$

The parameter U_∞/U_m can be thought of as a measure of the density difference between the fluid and the particle. Brenner (1966) identified five separtate flow regimes for this problem based on the magnitude of U_∞/U_m. For all 5 of these flow regimes, Brenner postulated that the the lateral migration velocity of the sphere should scale linearly with the tube Reynolds number, Re. The current results are best correlated to Brenner's case (iii) characterized by $(2a/D)^2 << |U_\infty|/U_m << 1$. These results contradict Brenner's conjecture in that the lateral migration velocity does not scale linearly with the tube Reynolds number.

Preliminary results were also obtained for the lateral migration of a spherical particle suspended in pressure-driven flow of a power-law fluid. The non-Newtonian behavior of the fluid was seen to greatly affect the migration velocity to the point where the direction of the migration can be reversed.

Acknowledgement: This work was partially supported by the U. S. Department of Energy (DOE) grants DE-FG03-97ER14778 and DE-FG03-97ER25332. This

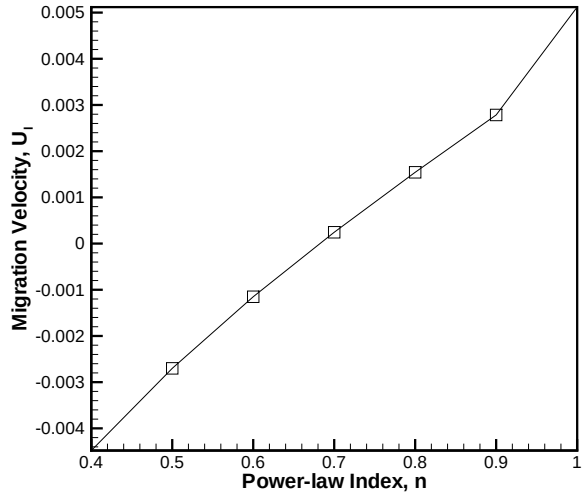

Figure 6 : The lateral migration velocity as a function of the power-law index n for the case in which the sphere leads the mean flow with $r = 0.7$ and $|U_\infty|/U_m$=0.14391.

financial support does not constitute an endorsement by the DOE of the views expressed in this paper.

References

Ahmad, S.; Banerjee, P. K. (1986): Free vibration analysis of BEM using particular integrals. *J. Engrg. Mech.*, vol. 112, pp. 682–695.

Brenner, H. (1966): Hydrodynamic resistance of particles at small Reynolds numbers. *Adv. Chem. Engr.*, vol. 6, pp. 287–438.

Chhabra, R. P. (1993): *Bubbles, Drops, and Particles in Non-Newtonian Fluids*. CRC Press, Boca Raton.

Cox, R. G.; Hsu, S. K. (1977): The lateral migration of solid particles in a laminar flow near a plane. *Int. J. Multiphase flow*, vol. 3, pp. 201–222.

Fang, Z.; Mammoli, A. A.; Ingber, M. S. (2001): Analyzing irreversibilities in Stokes flows containing suspended particles using the traction boundary integral equation method. *Engr. Anal. Bound. Elmnts.*, vol. 25, no. 4, pp. 249–257.

Golberg, M. A.; Chen, C. S.; Bowman, H.; Power, H. (1998): Some comments on the use of radial basis functions in the dual-reciprocity method. *Comp. Mech.*, vol. 21, no. 2, pp. 141–148.

Ho, B. P.; Leal, L. G. (1974): Inertial migration of rigid spheres in two-dimenstional unidirectional flows. *J. Fluid Mech.*, vol. 65, no. 2, pp. 365–400.

Ingber, M. S. (1991): Dynamic simulation of the hydrodynamic interaction among immersed particles in Stokes flow. *Int. J. Num. Meth. Fluids*, vol. 10, pp. 791–809.

Ingber, M. S.; Li, J. (1991): Surface pressure solution for boundary element analysis of Stokes flow. *Comm. Appl. Num. Meths.*, vol. 7, pp. 367–376.

Ingber, M. S.; Mammoli, A. A.; Brown, M. J. (2001): A comparison of domain integral evaluation techniques for boundary element methods. *Int. J. Numer. Meth. Engrg.*, vol. 52, no. 4, pp. 417–432.

Ingber, M. S.; Phan-Thien, N. (1992): A boundary element approach for parabolic equations using a calss of particular solutions. *Appl. Math. Mod.*, vol. 16, pp. 124–132.

Ishii, K.; Hasimoto, H. (1980): Lateral migration of a spherical particle in flows in a ciruclar tube. *J. Phys. Soc. Japan*, vol. 48, pp. 2144–2155.

Jeffrey, R. C.; Pearson, J. R. A. (1963): Particle motion in laminar vertical tube flow. *J. Fluid. Mech.*, vol. 22, pp. 721–735.

Ladyzhenskaya, G. A. (1963): *The Mathematical Theory of Incompressible Flow*. Gordon and Breach, New York.

Li, J.; Ingber, M. S. (1994): A numerical study of lateral migration of spherical particles in Poiseuille flow. *Engrg. Anal. Bound. Elmnts.*, vol. 13, no. 1, pp. 83–92.

Lin, H.; Atluri, S. N. (2001): The meshless local Petrov-Galerkin (MLPG) method for solving Incompressible Navier-Stokes equations. *CMES: Computer Modeling in Engineering & Sciences*, vol. 2, no. 2, pp. 117–142.

Nowak, A. J. (1989): The multiple reciprocity method of solving transient heat conduction problems. In Brebbia, C. A.; Connor, J. J.(Eds): *Advances in Boundary Elements*, pp. 81–93, Berlin. Springer-Verlag.

Partridge, P. W.; Wrobel, C. A. B. L. C. (1992): *The Dual Reciprocity Boundary Element Method*. Elsevier Applied Science, London.

Power, H. (1994): A complete multiple reciprocity approximation for the the non-permanent Stokes flow. In Brebbia, C. A.; Kassab, A. J.(Eds): *Boundary Element Technology IX*, pp. 127–137, Southampton.

Segré, G.; Silberberg, A. (1961): Radial particle displacements in Poiseuille flow of suspensions. *Nature*, vol. 189, pp. 209–210.

Tran-Cong, T.; Phan-Thien, N. (1989): Stokes problems of multiparticle systems: A numerical method for arbitrary flows. *Phys. Fluids A*, vol. 1, no. 3, pp. 453–461.

Tsai, C. C.; Young, D. L.; Cheng, A. H.-D. (2002): Meshless BEM for three-dimensional Stokes flows. *CMES: Computer Modeling in Engineering & Sciences*, vol. 3, no. 1, pp. 117–128.

Vasseur, P.; Cox, R. G. (1976): The lateral migration of a spherical particle in two-dimensional shear flows. *J. Fluid Mech.*, vol. 78, pp. 385–413.

Vasseur, P.; Cox, R. G. (1976): The lateral migration of spherical particles sedimenting in a stagnant bounded fluid. *J. Fluid Mech.*, vol. 80, pp. 561–591.